Thermal Fluctuations of Singular Bar-Joint Mechanisms

Manu Mannattil,[1,*] J. M. Schwarz,[1,2,†] and Christian D. Santangelo[1,‡]
[1]Department of Physics, Syracuse University, Syracuse, New York 13244, USA
[2]Indian Creek Farm, Ithaca, New York 14850, USA

(Received 8 December 2021; revised 1 March 2022; accepted 3 May 2022; published 20 May 2022)

A bar-joint mechanism is a deformable assembly of freely rotating joints connected by stiff bars. Here we develop a formalism to study the equilibration of common bar-joint mechanisms with a thermal bath. When the constraints in a mechanism cease to be linearly independent, singularities can appear in its shape space, which is the part of its configuration space after discarding rigid motions. We show that the free-energy landscape of a mechanism at low temperatures is dominated by the neighborhoods of points that correspond to these singularities. We consider two example mechanisms with shape-space singularities and find that they are more likely to be found in configurations near the singularities than others. These findings are expected to help improve the design of nanomechanisms for various applications.

DOI: 10.1103/PhysRevLett.128.208005

Introduction.—Bar-joint mechanisms constitute one of the simplest, widely employed models to understand a variety of mechanical structures ranging from viruses [1], colloidal clusters [2–5], crystals [6], and minerals [7], and robots and machines [8,9]. More recently, DNA origami has made the direct fabrication of miniaturized mechanisms possible at the nanoscale, where thermal fluctuations due to the surrounding medium cannot be neglected [10,11]. More generic examples of thermally driven mechanisms include ordered and disordered lattices [12–14], polymerized membranes [15,16], and polyhedral nets [17–19]. There is, therefore, an arising need to understand how thermal excitations affect the physical properties of these mechanisms, but only some attempts have been made so far [3,20].

The effect of thermal fluctuations on a physical system is often represented by its free-energy landscape in terms of collective variables that provide a coarse-grained description of its slowest dynamics. In theory [21,22], one can obtain the free energy of a mechanism by integrating out the fast modes that are transverse to its shape space, i.e., the subset of its configuration space once rigid-body motions are removed. Doing this, however, becomes nontrivial when the mechanism has shape-space singularities [9,23,24]. For concreteness, consider the shape space of the planar four-bar linkage with freely rotating joints [25–27] (Fig. 1). Though this linkage has one degree of freedom up to Euclidean motions, it has two modes of deformation, one where the angle $\theta_1 = \theta_2$ and another where $\theta_1 \neq \theta_2$, meeting at two isolated singular points $(\theta_1, \theta_2) = (0, 0)$ and (π, π). One generically expects the mechanism to be soft at these singularities, and indeed the free energy diverges in a harmonic approximation of the elastic energy [20]. These divergences must be cut off by higher-order nonlinear effects, yet how this happens and to what extent remains to be understood.

In this Letter, we develop a formalism to understand the thermal equilibration of common bar-joint mechanisms that have isolated shape-space singularities. We show that the divergent contributions to the free energy arising in the harmonic approximation to the energy are suppressed by anharmonic corrections. These findings show the existence of energetic free-energy barriers between configurations near the singularities and configurations farther from the singularities. Our results are consistent with a closely related work [3,4] on singular colloidal clusters, but allow for isolated singularities of the shape space. We demonstrate our results using both the four-bar linkage as well as a flat, triangulated origami [28]. Our analysis has direct consequences in the design and employment of nanoscale mechanisms in applications ranging from self-assembly [29] to drug delivery [30], where relative thermodynamic stability of different configurations is of paramount importance.

Mechanisms and singularities.—We consider bar-joint mechanisms made of $N \geq 3$ pointlike joints in d dimensions

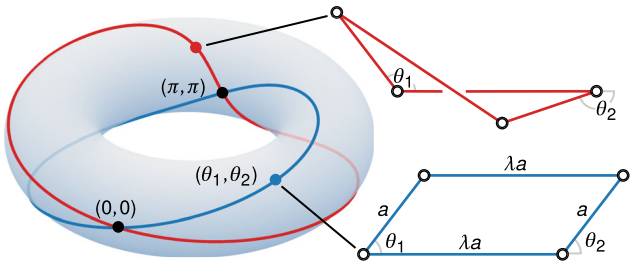

FIG. 1. Shape space of the planar four-bar linkage visualized as two intersecting curves on a torus, each curve representing a "branch" of the shape space. The poloidal and toroidal angles along the branches correspond to the angles θ_1 and θ_2 of the linkage, which has two modes of deformation with $\theta_1 = \theta_2$ (blue curve) and $\theta_1 \neq \theta_2$ (red curve).

connected by $m < Nd - \frac{1}{2}d(d+1)$ freely rotating, massless bars. If the joints have position vectors $\boldsymbol{r}_1, \boldsymbol{r}_2, \ldots, \boldsymbol{r}_N \in \mathbb{R}^d$ in the lab frame, the mechanism's configuration can be fully described at any given moment using a configuration vector $\boldsymbol{r} \in \mathbb{R}^{Nd}$ defined by $\boldsymbol{r} = (\boldsymbol{r}_1, \boldsymbol{r}_2, \ldots, \boldsymbol{r}_N)$. We assume the bars in the mechanism to be stiff but compressible with an energy that depends on the bar lengths so that the total energy of the mechanism is $U(\boldsymbol{r}) = \sum_{i=1}^{m} \phi_i[\ell_i(\boldsymbol{r})]$. Here $\ell_i(\boldsymbol{r})$ is the length of the ith bar with an energy $\phi_i(\ell_i)$, which is assumed to have a minimum value of zero at $\ell_i = \bar{\ell}_i$, the natural length of the ith bar.

With the above form of the energy, all nontrivial ground states of a mechanism belong to its shape space Σ [31–33], which is the set of all deformed configurations of the mechanism with the length of each bar equal to its natural length, once rotations and translations are removed. To practically identify Σ, we first switch to a Cartesian body frame attached to the mechanism so that all $\frac{1}{2}d(d+1)$ rigid motions are eliminated [22,34]. We require $n = Nd - \frac{1}{2}d(d+1)$ coordinates to specify the state of the mechanism in the body frame and let $\boldsymbol{q} \in \mathbb{R}^n$ be its configuration vector in this frame. Now consider m holonomic constraint functions $f_i : \mathbb{R}^n \to \mathbb{R}$, $i = 1, 2, \ldots, m$, each associated with a single bar, and defined by $f_i(\boldsymbol{q}) = [\ell_i^2(\boldsymbol{q}) - \bar{\ell}_i^2]/(2\bar{\ell}_i)$. The m scalar constraint functions can also be considered together as a single constraint map $f : \mathbb{R}^n \to \mathbb{R}^m$ defined by $f(\boldsymbol{q}) = [f_1(\boldsymbol{q}), f_2(\boldsymbol{q}), \ldots, f_m(\boldsymbol{q})]$. Then, the shape space is the zero level set $\Sigma = \{\boldsymbol{q} \in \mathbb{R}^n : f(\boldsymbol{q}) = \boldsymbol{0}\}$. In the absence of external forces, each point in Σ is a ground-state configuration of the mechanism with a distinct shape.

The compatibility matrix $\mathsf{C}(\boldsymbol{q})$ [35,36] at a configuration $\boldsymbol{q} \in \Sigma$ is the $m \times n$ Jacobian matrix ∇f of the constraint map f. If C has full rank for all points in Σ, then Σ is an $(n-m)$-dimensional submanifold of $\mathbb{R}^n$ [37,38]. When Σ has a "branched" structure, e.g., like in Fig. 1, $\mathsf{C}(\boldsymbol{q})$ drops rank at the singularity where the branches meet [39,40], and the constraints cease to be linearly independent. Such singularities are the most common singularities [39,41] found in a mechanism and here we consider the situation where they occur only at isolated points of Σ. (For other, less common singularities that can occur in a mechanism, see Refs. [39,40,42], and references therein.) The branches of Σ, being $(n-m)$-dimensional submanifolds of $\mathbb{R}^n$, can be individually parametrized using a set of coordinates $\xi \in \mathbb{R}^{n-m}$, called shape coordinates [43] as they capture the shape changes of the mechanism as it moves on Σ. We also assume that n is small enough that such parametrizations can be found without much difficulty and that the branches are linearly independent at the singularity [39]. Zero-energy shape changes constitute the slowest dynamics in a mechanism, so it follows that the shape coordinates ξ are the most natural collective variables (CVs) for a low-dimensional description of a thermally excited mechanism.

Thermal fluctuations.—Let us assume that the value of the chosen CV for any configuration $\boldsymbol{q} \in \mathbb{R}^n$ of the mechanism can be measured using the CV map $\hat{\xi}(\boldsymbol{q})$. [In the case of the four-bar linkage, for example, if we choose θ_1 as the CV, then $\hat{\xi}(\boldsymbol{q})$ is the map that computes θ_1 for any $\boldsymbol{q}$, whether or not it lies on the branches of the linkage's shape space.] The free energy associated with the CV ξ is [44]

$$\mathcal{A}_{\hat{\xi}}(\xi) = -\beta^{-1} \ln \mathcal{P}_{\hat{\xi}}(\xi), \tag{1}$$

where β is the inverse temperature and $\mathcal{P}_{\hat{\xi}}(\xi)$ is the marginal probability density of the CV, which, aside from factors of normalization, is

$$\mathcal{P}_{\hat{\xi}}(\xi) = \int_{\mathbb{R}^n} d\boldsymbol{q} I(\boldsymbol{q}) \delta[\hat{\xi}(\boldsymbol{q}) - \xi] \exp[-\beta U(\boldsymbol{q})]. \tag{2}$$

Here $\delta[\cdot]$ is the $(n-m)$-dimensional Dirac delta function, which restricts the domain of integration to the m-dimensional CV level set $\hat{\xi}^{-1}(\xi) = \{\boldsymbol{q} \in \mathbb{R}^n : \hat{\xi}(\boldsymbol{q}) = \xi\}$ [45], and $I(\boldsymbol{q})$ is a Jacobian factor introduced by the change of coordinates from the lab frame to the body frame. When $\hat{\xi}$ has full rank in $\hat{\xi}^{-1}(\xi)$, the coarea formula [44] lets us express $\mathcal{P}_{\hat{\xi}}(\xi)$ as an exact high-dimensional surface integral over $\hat{\xi}^{-1}(\xi)$, but evaluating it is a difficult task in practice. Hence, we resort to asymptotic methods for its evaluation.

At low temperatures (i.e., large β) we can asymptotically evaluate the integral in Eq. (2) by expanding the energy $U(\boldsymbol{q})$ around the ground-state configurations in $\hat{\xi}^{-1}(\xi)$. Since all ground states belong to the shape space Σ, they could be regular (i.e., nonsingular) points or singularities of Σ. We call ξ a regular value of the CV if $\hat{\xi}^{-1}(\xi)$ does not contain singularities of Σ and vice versa. For now, let us assume that ξ is a regular value of the CV and that $\hat{\xi}^{-1}(\xi)$ contains just one ground state $\bar{\boldsymbol{q}}$. If $\boldsymbol{q}$ is a point near $\bar{\boldsymbol{q}}$, after setting $\boldsymbol{q} \to \bar{\boldsymbol{q}} + \boldsymbol{q}$, we expand the energy to the lowest order around $\bar{\boldsymbol{q}}$ and find the harmonic energy $U \approx \frac{1}{2}\boldsymbol{q}^{\mathsf{T}}\mathsf{C}^{\mathsf{T}}\mathsf{K}\mathsf{C}\boldsymbol{q} = \frac{1}{2}\boldsymbol{q}^{\mathsf{T}}\mathsf{D}\boldsymbol{q}$. Here $\mathsf{D} = \mathsf{C}^{\mathsf{T}}\mathsf{K}\mathsf{C}$ is the dynamical matrix evaluated at $\bar{\boldsymbol{q}}$ [36] (assuming joints of unit mass) and K is the diagonal matrix of bar stiffnesses $\phi_i''(\bar{\ell}_i)$, which we set equal to κ for all bars for simplicity. See the Supplemental Material [46] for details. Since $\bar{\boldsymbol{q}}$ is a regular point of Σ, C has full rank, and D has $n-m$ independent zero modes that belong to $\ker \mathsf{C} = \{\boldsymbol{u} \in \mathbb{R}^n : \mathsf{C}\boldsymbol{u} = \boldsymbol{0}\}$ [36]. These zero modes are all tangent to Σ and represent a degree of freedom [37]. Hence, to asymptotically evaluate Eq. (2) in the neighborhood of a regular point, we can safely use the harmonic approximation since any divergence [20,63,64] due to these zero modes is regularized by the delta function, which suppresses all contributions to the integral that are tangent to Σ [65]. Then, the asymptotic marginal density for a regular value ξ of the CV is (Supplemental Material [46])

$$\mathcal{P}_{\hat{\xi}}(\xi) \sim I(\xi) \left(\frac{2\pi}{\beta}\right)^{m/2} \left| \frac{\det[\nabla\psi(\xi)]^{\mathsf{T}}\nabla\psi(\xi)}{\det \mathsf{D}^{\perp}(\xi)} \right|^{1/2}. \tag{3}$$

Here $\psi:\mathbb{R}^{n-m}\to\mathbb{R}^n$ is a parameterization of Σ near $\bar{\boldsymbol{q}}\in\Sigma$ in terms of the CV ξ, and compatible with the CV map, such that $\bar{\boldsymbol{q}}=\psi(\xi)$ and $\hat{\xi}(\bar{\boldsymbol{q}})=\xi$. Also, $\det(\nabla\psi)^{\mathsf{T}}\nabla\psi$ is the determinant of the induced metric on Σ and $\mathsf{D}^{\perp}$ is the diagonal matrix of the m nonzero eigenvalues of D at $\bar{\boldsymbol{q}}$.

Now, consider the situation at a shape-space singularity, where C has rank deficiency. At such a point, using the Maxwell-Calladine count [66,67], we find that the number of zero modes increases to $n-m+s$, where s is the number of independent self stresses $\boldsymbol{\sigma}\in\ker\mathsf{C}^{\mathsf{T}}$—each self stress being a set of bar tensions that leave the mechanism in equilibrium [36]. The zero modes at a singularity are not all tangent to Σ, which means that the delta function in Eq. (2) fails to suppress the divergences due to these zero modes when the harmonic approximation is used. Furthermore, as one approaches the singularity along Σ, the lowest s nonzero eigenvalues of the dynamical matrix D become small leading to an effective softening of the mechanism. This causes Eq. (3) to break down even for regular ground states in the vicinity of the singularity. For instance, for the four-bar linkage, using Eq. (3) we find $\mathcal{P}_{\hat{\theta}_1}(\theta_1)\sim|\sin\theta_1|^{-1}$ (Supplemental Material [46]), which diverges as $\theta_1\to 0,\pm\pi$.

To resolve the problem, we need to consider higher-order contributions to the energy due to the excess zero modes at the singularity. Consider a singularity $\bar{\boldsymbol{q}}^*\in\Sigma$, where the CV has the value ξ^*. For now, let us also assume that the only ground state in the CV level set $\hat{\xi}^{-1}(\xi^*)$ is $\bar{\boldsymbol{q}}^*$. For a point $\boldsymbol{q}$ close to $\bar{\boldsymbol{q}}^*\in\Sigma$, we set $\boldsymbol{q}\to\bar{\boldsymbol{q}}^*+\boldsymbol{q}$ and write $\boldsymbol{q}=\boldsymbol{u}+\boldsymbol{v}$. Here $\boldsymbol{u}\in\ker\mathsf{C}$ is a zero mode, $\boldsymbol{v}\in(\ker\mathsf{C})^{\perp}$ is a fast vibrational mode of the system, and $(\ker\mathsf{C})^{\perp}$ is the orthogonal complement of $\ker\mathsf{C}$ in $\mathbb{R}^n$. Expanding the energy to the lowest order in $\boldsymbol{u}$ and $\boldsymbol{v}$ around $\bar{\boldsymbol{q}}^*$ [3,12,13] we find (Supplemental Material [46])

$$U\approx\frac{1}{2}[\mathsf{C}\boldsymbol{v}+\boldsymbol{w}(\boldsymbol{u})]^{\mathsf{T}}\mathsf{K}[\mathsf{C}\boldsymbol{v}+\boldsymbol{w}(\boldsymbol{u})]. \tag{4}$$

Here $\boldsymbol{w}(\boldsymbol{u})\in\mathbb{R}^m$ is a vector such that its ith component is $\frac{1}{2}\boldsymbol{u}^{\mathsf{T}}\nabla\nabla f_i\boldsymbol{u}$, with $\nabla\nabla f_i$ being the Hessian matrix of the ith constraint function f_i, evaluated at $\bar{\boldsymbol{q}}^*$. This makes the above energy expansion quartic in the zero modes $\boldsymbol{u}$.

Equation (4) is only valid when the expansion is around the singularity $\bar{\boldsymbol{q}}^*$, and a similar expansion does not exist for ground states in $\hat{\xi}^{-1}(\xi)$ for ξ close to ξ^*, where the harmonic approximation is not applicable either. Thus, for $\xi\to\xi^*$, we choose to find $\mathcal{P}_{\hat{\xi}}(\xi)$ by directly evaluating the integral over $\hat{\xi}^{-1}(\xi)$ using the coarea formula. To simplify the evaluation, we make two assumptions: (i) for points close to $\bar{\boldsymbol{q}}^*$, the CV map $\hat{\xi}$ can be approximated by its Taylor expansion around $\bar{\boldsymbol{q}}^*$: $\hat{\xi}=\xi^*+(\nabla\hat{\xi})\boldsymbol{q}+\mathcal{O}(\|\boldsymbol{q}\|^2)$, with $\nabla\hat{\xi}$ being the Jacobian matrix of $\hat{\xi}$ at $\bar{\boldsymbol{q}}^*$; (ii) fast modes that belong to $(\ker\mathsf{C})^{\perp}$ do not change the value of the CV to linear order at $\bar{\boldsymbol{q}}^*$, i.e., $(\nabla\hat{\xi})\boldsymbol{v}=\boldsymbol{0}$. Assumption (i) linearizes the CV map and turns its level sets near the singularity into hyperplanes, simplifying the evaluation of Eq. (2). Although assumption (ii) is stringent on the shape coordinate we use as the CV, it is true for most reasonable choices and a good CV should mainly be sensitive to the slow modes [68]. This makes it possible to use the quartic energy expansion and integrate over the fast modes. Note that in the above steps, we do not make use of any parametrization of Σ, unlike in Eq. (3).

Using the linearized CV map and the quartic expansion for the energy [Eq. (4)] in Eq. (2), we integrate out the fast vibrational modes $\boldsymbol{v}$ to find (Supplemental Material [46])

$$\mathcal{P}_{\hat{\xi}}(\xi)\sim\frac{I(\xi^*)}{|\det\mathsf{D}^{\perp}\det\nabla\hat{\xi}(\nabla\hat{\xi})^{\mathsf{T}}|^{1/2}}\left(\frac{2\pi}{\beta}\right)^{(m-s)/2}\times\int_{\Xi_\xi}d\Omega(\boldsymbol{u})\exp\left\{-\frac{1}{2}\beta\kappa\sum_{\boldsymbol{\sigma}}[\boldsymbol{\sigma}\cdot\boldsymbol{w}(\boldsymbol{u})]^2\right\},\quad\xi\to\xi^*, \tag{5}$$

where $\boldsymbol{\sigma}\in\ker\mathsf{C}^{\mathsf{T}}$ are the self stresses and $\mathsf{D}^{\perp}$ is the diagonal matrix of the $m-s$ nonzero eigenvalues of D at $\bar{\boldsymbol{q}}^*$. Also, $d\Omega(\boldsymbol{u})$ is the area element on the integration domain Ξ_ξ, which is geometrically an s-dimensional hyperplane formed by the intersection of $\ker\mathsf{C}$ and the level set of the linearized CV map $(\nabla\hat{\xi})^{-1}(\xi-\xi^*)=\{\boldsymbol{u}\in\mathbb{R}^n:\xi^*+(\nabla\hat{\xi})\boldsymbol{u}=\xi\}$. On choosing a basis for $\ker\mathsf{C}$, the term in the exponential of the above integral becomes a quartic polynomial, making further simplification difficult. We discuss the convergence criteria for Eq. (5) in the Supplemental Material [46].

On the basis of how $\mathcal{P}_{\hat{\xi}}(\xi)$ in Eqs. (3) and (5) scales with β, we can show that the free-energy barriers between regular and singular values of the CV have a temperature and stiffness dependence $\sim\ln\beta\kappa$, making the barriers energetic in nature. This is not surprising considering the overall softening of the mechanism near the singularities. Also, for both the quartic and harmonic approximations for $\mathcal{P}_{\hat{\xi}}(\xi)$, we expect the range of validity (in ξ) to increase with increasing β, along with an increase in the range where both approximations produce similar results.

So far we have only considered cases where the CV level set $\hat{\xi}^{-1}(\xi)$ contains only one regular point or a singularity of Σ. However, as Σ has a branched structure, ξ need not identify a configuration in Σ uniquely. Indeed, for the four-bar linkage, we see that there are as many as two configurations with a given value of θ_1 (Fig. 1). Nonetheless, it is easy to find the asymptotic marginal density for more general cases by using combinations of Eqs. (3) and (5) to add the contribution of each ground state in $\hat{\xi}^{-1}(\xi)$ individually, noting that Eq. (5) gives the collective contribution from all the branches meeting at a singularity.

Examples and discussion.—We now use our formalism to find the free-energy profiles of two example mechanisms with one-dimensional shape spaces with isolated singularities and compare them with results from Monte Carlo

simulations. (Also see the Supplemental Material [46] for an example mechanism with a two-dimensional shape space and a mechanism with a permanent state of self stress, which is unlike the case where it appears only at isolated singularities.) Motivated by typical DNA origami structures that have lengths in the range of a few hundred nanometers with stiffness in the range 0.1–1 pN/nm [11], we choose a nondimensional inverse temperature of $\beta = 10^4$ and use a potential of the form $\phi_i(\ell_i) = (\ell_i^2 - \bar{\ell}_i^2)^2/(8\bar{\ell}_i^2)$ so that $\phi_i''(\bar{\ell}_i) = \kappa = 1$. Further details on the simulations are given in the Supplemental Material [46].

The four-bar linkage we consider (Fig. 1) is made out of two sets of bars of lengths a and λa, where $\lambda > 0$ is a dimensionless aspect ratio. For $\lambda \neq 1$, the linkage has shape-space singularities at $\theta_1 = 0$ and $\theta_1 = \pm\pi$ where the bars become collinear and support a state of self stress. [For simplicity, we do not discuss the square four-bar linkage with $\lambda = 1$ in this Letter as it has additional singularities at $(\theta_1, \theta_2) = (0, \pm\pi)$ [69]]. The shape space can be fully parameterized using the angle θ_1, which we use as our CV and choose $\theta_1 = 0$ as the point of zero free energy. For θ_1 far from the singular values we use Eq. (3) to find the free-energy difference $\Delta\mathcal{A}_{\hat{\theta}_1}(\theta_1) = \mathcal{A}_{\hat{\theta}_1}(\theta_1) - \mathcal{A}_{\hat{\theta}_1}(0)$ as (Supplemental Material [46])

$$\Delta\mathcal{A}_{\hat{\theta}_1}(\theta_1) \sim \beta^{-1} \ln[X^{1/2} D_{-1/2}(0) |\sin\theta_1|], \quad 0 \ll |\theta_1| \ll \pi, \tag{6}$$

where $D_{-1/2}(\cdot)$ is the parabolic cylinder function [70] and $X = \sqrt{\beta\kappa}\lambda a/(8|\lambda - 1|)$ is a dimensionless term that is independent of θ_1. As expected, Eq. (6) diverges when θ_1 is close to the singular values $\theta_1 = 0$ or $\theta_1 = \pm\pi$. For $\theta_1 \to 0$, using Eq. (5), the free-energy difference takes the form (Supplemental Material [46])

$$\Delta\mathcal{A}_{\hat{\theta}_1}(\theta_1) \sim \beta^{-1} \left\{ X^2\theta_1^4 - \ln\left[\frac{D_{-1/2}(-2X\theta_1^2)}{D_{-1/2}(0)}\right] \right\}, \quad \theta_1 \to 0. \tag{7}$$

A similar expression is derived in the Supplemental Material [46] for $\theta \to \pm\pi$. A comparison between the numerical results and asymptotic expressions in Eqs. (6) and (7) (Fig. 2) shows excellent agreement for all values of θ_1.

For further testing our methods, we consider an origami made by triangulating a unit square [28] and embedded in three dimensions [Fig. 3(a)]. To make the origami more realistic, in simulations, we avoid all configurations that result in face intersections. The one-dimensional shape space [Fig. 3(b)] of this origami can be visualized as four intersecting branches in the space of the fold angles, i.e., the supplement of the dihedral angle at a fold. The intersection point is the singular flat state of the origami, where all the fold angles are zero. After numerically parametrizing the branches of the shape space in terms of the fold angle ρ_1, which we use as our CV, we utilize Eq. (3) to find the free energy $\mathcal{A}_{\hat{\rho}_1}(\rho_1)$ for $|\rho_1| \gg 0$. We next find $\mathcal{A}_{\hat{\rho}_1}(\rho_1)$ as $\rho_1 \to 0$ using Eq. (5) and choose $\rho_1 = 0$ as the point of zero free energy. A comparison between the numerical and the asymptotic results for the free-energy difference $\Delta\mathcal{A}_{\hat{\rho}_1}(\rho_1)$ shows good agreement in both regimes of ρ_1 [Fig. 3(c)]. Self-avoidance of the faces forces us to consider only a part of each branch of the shape space for our analysis. Since the extent of these parts (in ρ_1) vary for the four branches [Fig. 3(b)], it results in discontinuous jumps in the free-energy curves.

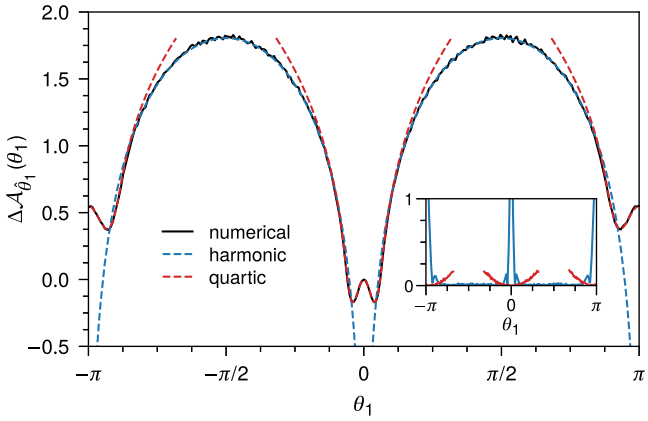

FIG. 2. Free-energy difference $\Delta\mathcal{A}_{\hat{\theta}_1}(\theta_1)$ of a four-bar linkage with parameters $a = 1$ and $\lambda = 2$ in units of β^{-1} at $\beta = 10^4$. The inset shows the absolute errors between the numerical and asymptotic results using the harmonic approximation [Eq. (6), blue curve] and quartic approximation [Eq. (7), red curves].

The free-energy landscapes of the four-bar linkage and the triangulated origami [Figs. 2 and 3(c)] demonstrate that the measured values of the CV tend to be closer to their values near the singularities. Yet, as free-energy landscapes (and even their extrema) do not always have a CV-agnostic interpretation [71–73], to draw conclusions we should also consider the physical meaning of the chosen CV. The CVs we picked for both the example mechanisms were internal angles whose values dictate the overall shape of the mechanism. Specifically, according to our results, we expect the bars of the four-bar linkage to tend to be collinear, as measured by the angle θ_1 being close to 0 or π. Similarly, the origami will tend towards being flat, as measured by the fold angle ρ_1. This tendency increases at lower temperatures as the free-energy barriers become larger. Finally, we remark on the apparent double-well nature of the landscapes near singular values of the CV. Because of the branched nature of the shape spaces, when $\theta_1 \to 0, \pm\pi$ or when $\rho_1 \to 0$, there are multiple ground states where the mechanism is also relatively soft. This is illustrated by the widening of the sublevel sets of the energy as one moves away from the singularity (e.g., see Fig. S4 in the Supplemental Material [46]). The net result is an increase in the number of thermodynamically favorable

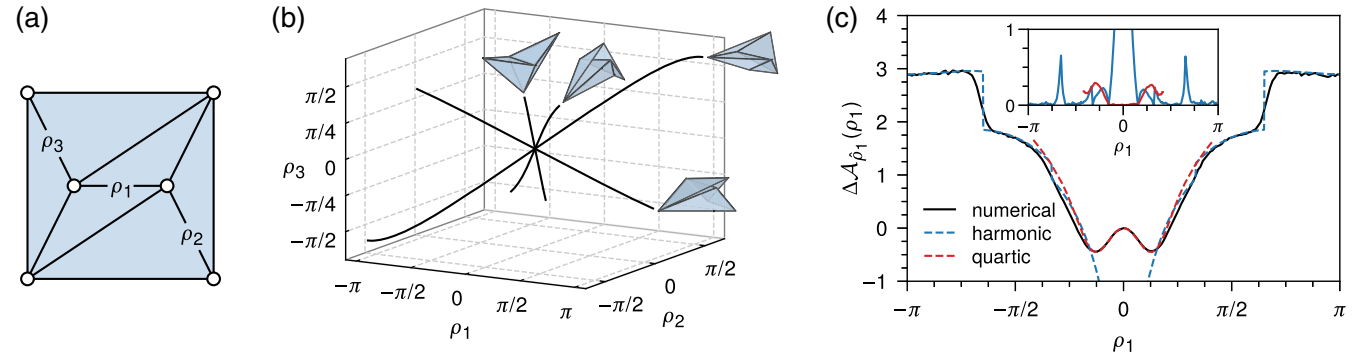

FIG. 3. (a) A triangulated origami modeled as a bar-joint mechanism and (b) its shape space visualized in the space of fold angles ρ_1, ρ_2, and ρ_3. (c) Free-energy difference $\Delta\mathcal{A}_{\hat{\rho}_1}(\rho_1)$ in units of β^{-1} at $\beta = 10^4$. The inset shows the absolute errors between the numerical and asymptotic results using the harmonic and quartic approximations (blue and red curves, respectively).

states with θ_1 close to 0 or $\pm\pi$ (and ρ_1 close to 0), causing an apparent lowering of the free energy.

Conclusion.—In this Letter we have described a formalism to find the free-energy landscapes of common bar-joint mechanisms with isolated singularities in their shape spaces. Our results indicate that configurations in the neighborhood of the singularities have relatively lower free energy compared to configurations farther from the singularities. This could help in programming the conformational dynamics of nanomechanisms [74]. Our findings also highlight the interplay between the geometry of a mechanism's shape space and its thermodynamic properties. Open questions include the behavior of these mechanisms in the thermodynamic limit [75,76], where configuration-space topology is often known to play a role [77], their behavior in the presence of active (nonthermal) noise [13], and methods to bias their dynamics towards desired states [78], e.g., by introducing CV-dependent bias potentials [79].

We acknowledge useful conversations with Xiaoming Mao and Zeb Rocklin. We also thank the anonymous reviewers for a careful reading of our manuscript. This work has been supported by the NSF Grants No. DMR-1822638 and No. DMR-1832002.

*mmannatt@syr.edu
†jmschw02@syr.edu
‡cdsantan@syr.edu

[1] B. M. Hespenheide, D. J. Jacobs, and M. F. Thorpe, Structural rigidity in the capsid assembly of cowpea chlorotic mottle virus, J. Phys. Condens. Matter **16**, S5055 (2004).
[2] M. Holmes-Cerfon, S. J. Gortler, and M. P. Brenner, A geometrical approach to computing free-energy landscapes from short-ranged potentials, Proc. Natl. Acad. Sci. U.S.A. **110**, E5 (2013).
[3] Y. Kallus and M. Holmes-Cerfon, Free energy of singular sticky-sphere clusters, Phys. Rev. E **95**, 022130 (2017).
[4] M. Holmes-Cerfon, Sticky-sphere clusters, Annu. Rev. Condens. Matter Phys. **8**, 77 (2017).
[5] J. F. Robinson, F. Turci, R. Roth, and C. P. Royall, Morphometric Approach to Many-Body Correlations in Hard Spheres, Phys. Rev. Lett. **122**, 068004 (2019).
[6] S. C. Power, Polynomials for crystal frameworks and the rigid unit mode spectrum, Phil. Trans. R. Soc. A **372**, 20120030 (2014).
[7] V. Kapko, C. Dawson, I. Rivin, and M. M. J. Treacy, Density of Mechanisms within the Flexibility Window of Zeolites, Phys. Rev. Lett. **107**, 164304 (2011).
[8] M. Farber, *Invitation to Topological Robotics* (European Mathematical Society, Zurich, 2008).
[9] P. S. Donelan, Singularity-theoretic methods in robot kinematics, Robotica **25**, 641 (2007).
[10] A. E. Marras, L. Zhou, H.-J. Su, and C. E. Castro, Programmable motion of DNA origami mechanisms, Proc. Natl. Acad. Sci. U.S.A. **112**, 713 (2015).
[11] W.-H. Jung, E. Chen, R. Veneziano, S. Gaitanaros, and Y. Chen, Stretching DNA origami: Effect of nicks and Holliday junctions on the axial stiffness, Nucl. Acids Res. **48**, 12407 (2020).
[12] L. Zhang and X. Mao, Finite-temperature mechanical instability in disordered lattices, Phys. Rev. E **93**, 022110 (2016).
[13] F. G. Woodhouse, H. Ronellenfitsch, and J. Dunkel, Autonomous Actuation of Zero Modes in Mechanical Networks Far from Equilibrium, Phys. Rev. Lett. **121**, 178001 (2018).
[14] L. Yan, Entropy favors heterogeneous structures of networks near the rigidity threshold, Nat. Commun. **9**, 1359 (2018).
[15] P. Di Francesco, Folding and coloring problems in mathematics and physics, Bull. Am. Math. Soc. **37**, 251 (2000).
[16] D. Nelson, T. Piran, and S. Weinberg, *Statistical Mechanics of Membranes and Surfaces*, 2nd ed. (World Scientific, Singapore, 2004).
[17] V. B. Shenoy and D. H. Gracias, Self-folding thin-film materials: From nanopolyhedra to graphene origami, MRS Bull. **37**, 847 (2012).
[18] P. M. Dodd, P. F. Damasceno, and S. C. Glotzer, Universal folding pathways of polyhedron nets, Proc. Natl. Acad. Sci. U.S.A. **115**, E6690 (2018).

[19] H. P. M. Melo, C. S. Dias, and N. A. M. Araújo, Optimal number of faces for fast self-folding kirigami, Comm. Phys. **3**, 154 (2020).

[20] D. Z. Rocklin, V. Vitelli, and X. Mao, Folding mechanisms at finite temperature, arXiv:1802.02704.

[21] N. Gō and H. A. Scheraga, On the use of classical statistical mechanics in the treatment of polymer chain conformation, Macromolecules **9**, 535 (1976).

[22] P. Echenique, C. N. Cavasotto, and P. García-Risueño, The canonical equilibrium of constrained molecular models, Eur. Phys. J. Spec. Top. **200**, 5 (2011).

[23] D. Zlatanov, I. A. Bonev, and C. M. Gosselin, Constraint singularities as C-space singularities, in *Advances in Robot Kinematics*, edited by J. Lenarčič and F. Thomas (Springer, Dordrecht, 2002), pp. 183–192.

[24] G. Liu, Y. Lou, and Z. Li, Singularities of parallel manipulators: a geometric treatment, IEEE Trans. Robot. Autom. **19**, 579 (2003).

[25] F. Grashof, *Theoretische Maschinenlehre* (Voss, Leipzig, 1883).

[26] R. Hartenberg and J. Danavit, *Kinematic Synthesis of Linkages* (McGraw-Hill, New York, 1964).

[27] D. Shimamoto and C. Vanderwaart, Spaces of polygons in the plane and Morse theory, Am. Math. Mon. **112**, 289 (2005).

[28] Bryan Gin-ge Chen and C. D. Santangelo, Branches of Triangulated Origami Near the Unfolded State, Phys. Rev. X **8**, 011034 (2018).

[29] T. Liedl, B. Högberg, J. Tytell, D. E. Ingber, and W. M. Shih, Self-assembly of three-dimensional prestressed tensegrity structures from DNA, Nat. Nanotechnol. **5**, 520 (2010).

[30] S. Zhao, F. Duan, S. Liu, T. Wu, Y. Shang, R. Tian, J. Liu, Z.-G. Wang, Q. Jiang, and B. Ding, Efficient intracellular delivery of RNase A using DNA origami carriers, ACS Appl. Mater. Interfaces **11**, 11112 (2019).

[31] D. G. Kendall, A survey of the statistical theory of shape, Stat. Sci. **4**, 87 (1989).

[32] P. G. Mezey, *Shape in Chemistry* (Wiley-VCH, New York, NY, 1993).

[33] *Shape & Shape Theory*, edited by D. G. Kendall, D. Barden, T. K. Carne, and H. Le (John Wiley & Sons, Ltd., Chichester, 1999).

[34] D. R. Herschbach, H. S. Johnston, and D. Rapp, Molecular partition functions in terms of local properties, J. Chem. Phys. **31**, 1652 (1959).

[35] S. Pellegrino and C. Calladine, Matrix analysis of statically and kinematically indeterminate frameworks, Int. J. Solids Struct. **22**, 409 (1986).

[36] T. C. Lubensky, C. L. Kane, X. Mao, A. Souslov, and K. Sun, Phonons and elasticity in critically coordinated lattices, Rep. Prog. Phys. **78**, 073901 (2015).

[37] B. Leimkuhler and S. Reich, *Simulating Hamiltonian Dynamics* (Cambridge University Press, Cambridge, England, 2005).

[38] J. M. Lee, *Introduction to Smooth Manifolds*, 2nd ed. (Springer, New York, NY, 2013).

[39] P. López-Custodio, A. Müller, X. Kang, and J. Dai, Tangential intersection of branches of motion, Mech. Mach. Theory **147**, 103730 (2020).

[40] *Singular Configurations of Mechanisms and Manipulators*, edited by A. Müller and D. Zlatanov (Springer, Cham, 2019).

[41] P. López-Custodio, A. Müller, J. Rico, and J. Dai, A synthesis method for 1-DOF mechanisms with a cusp in the configuration space, Mech. Mach. Theory **132**, 154 (2019).

[42] A. Müller, Higher-order analysis of kinematic singularities of lower pair linkages and serial manipulators, J. Mech. Robot. **10**, 011008 (2017).

[43] R. G. Littlejohn and M. Reinsch, Internal or shape coordinates in the n-body problem, Phys. Rev. A **52**, 2035 (1995).

[44] T. Lelièvre, M. Rousset, and G. Stoltz, *Free Energy Computations: A Mathematical Perspective* (Imperial College Press, London, 2010).

[45] C. Hartmann, J. C. Latorre, and G. Ciccotti, On two possible definitions of the free energy for collective variables, Eur. Phys. J. Spec. Top. **200**, 73 (2011).

[46] See Supplemental Material at http://link.aps.org/supplemental/10.1103/PhysRevLett.128.208005, which includes Refs. [47–62], for derivations of (i) lowest-order approximation of the energy [Eq. (4)], (ii) asymptotic expressions for the marginal probability density [Eqs. (3) and (5)], and (iii) free energy of the four-bar linkage [Eqs. (6) and (7)], as well as further discussions on (iv) the origami, (v) the five-bar linkage (a mechanism with a two-dimensional shape space), (vi) mechanisms with a permanent state of self stress, and (vii) the numerical simulations.

[47] P. Diaconis, S. Holmes, and M. Shahshahani, Sampling from a Manifold, in *Advances in Modern Statistical Theory and Applications*, Collections Vol. 10 (Institute of Mathematical Statistics, Beachwood, OH, 2013), pp. 102–125.

[48] K. W. Breitung, *Asymptotic Approximations for Probability Integrals* (Springer, Berlin, 1994).

[49] C. Hartmann, Model reduction in classical molecular dynamics, Ph.D. thesis, Freie Universität Berlin, 2007.

[50] R. Connelly and H. Servatius, Higher-order rigidity—what is the proper definition?, Discrete Comput. Geom. **11**, 193 (1994).

[51] R. Connelly and W. Whiteley, Second-order rigidity and prestress stability for tensegrity frameworks, SIAM J. Discrete Math. **9**, 453 (1996).

[52] W. O. Williams, A primer on the mechanics of tensegrity structures, Technical Report, Center for Nonlinear Analysis, Department of Mathematical Sciences, Carnegie Mellon University, Pittsburgh, PA, 2003, https://www.math.cmu.edu/~wow/papers/newprimer.pdf.

[53] L. Wu, A. Müller, and J. S. Dai, A matrix method to determine infinitesimally mobile linkages with only first-order infinitesimal mobility, Mech. Mach. Theory **148**, 103776 (2020).

[54] H. Whitney, Tangents to an analytic variety, Ann. Math. **81**, 496 (1965).

[55] P. A. M. Dirac, *The Principles of Quantum Mechanics*, 4th ed. (Oxford University Press, London, 1958).

[56] T. Tarnai, Kinematic bifurcation, in *Deployable Structures*, edited by S. Pellegrino (Springer, Vienna, 2001), Chap. 8, pp. 143–169.

[57] O. Mermoud and M. Steiner, Visualisation of configuration spaces of polygonal linkages, J. Geom. Graph. **4**, 147 (2000).
[58] R. Curtis and M. Steiner, Configuration spaces of planar pentagons, Am. Math. Mon. **114**, 183 (2007).
[59] M. Kapovich and J. Millson, On the moduli space of polygons in the Euclidean plane, J. Diff. Geom. **42**, 430 (1995).
[60] M. Berry, M. E. Lee-Trimble, and C. D. Santangelo, Topological transitions in the configuration space of non-Euclidean origami, Phys. Rev. E **101**, 043003 (2020).
[61] O. Tropp, A. Tal, and I. Shimshoni, A fast triangle to triangle intersection test for collision detection, Comp. Anim. Virtual Worlds **17**, 527 (2006).
[62] https://github.com/manu-mannattil/thermmech.
[63] A. S. Schwarz, Instantons and fermions in the field of instanton, Commun. Math. Phys. **64**, 233 (1979).
[64] R. S. Ellis and J. S. Rosen, Asymptotic analysis of Gaussian integrals, II: Manifold of minimum points, Commun. Math. Phys. **82**, 153 (1981).
[65] P. Ramond, *Field Theory: A Modern Primer* (Westview Press, Boulder, CO, 1997).
[66] J. C. Maxwell, On the calculation of the equilibrium and stiffness of frames, Philos. Mag. **27**, 294 (1864).
[67] C. Calladine, Buckminster Fuller's "tensegrity" structures and Clerk Maxwell's rules for the construction of stiff frames, Int. J. Solids Struct. **14**, 161 (1978).
[68] P. Tiwary and B. J. Berne, Spectral gap optimization of order parameters for sampling complex molecular systems, Proc. Natl. Acad. Sci. U.S.A. **113**, 2839 (2016).
[69] R. Yang and P. S. Krishnaprasad, On the geometry and dynamics of floating four-bar linkages, Dyn. Stab. Syst. **9**, 19 (1994).
[70] *NIST Handbook of Mathematical Functions*, edited by F. W. J. Olver, D. W. Lozier, R. F. Boisvert, and C. W. Clark (Cambridge University Press, New York, NY, 2010).
[71] W. E and E. Vanden-Eijnden, Metastability, conformation dynamics, and transition pathways in complex systems, in *Multiscale Modelling and Simulation*, edited by S. Attinger and P. Koumoutsakos (Springer, Berlin, 2004), pp. 35–68.
[72] C. Hartmann and C. Schütte, Comment on two distinct notions of free energy, Physica (Amsterdam) **228D**, 59 (2007).
[73] D. Frenkel, Simulations: The dark side, Eur. Phys. J. Plus **128**, 10 (2013).
[74] K. E. Dunn, F. Dannenberg, T. E. Ouldridge, M. Kwiatkowska, A. J. Turberfield, and J. Bath, Guiding the folding pathway of DNA origami, Nature (London) **525**, 82 (2015).
[75] F. F. Abraham and D. R. Nelson, Fluctuations in the flat and collapsed phases of polymerized membranes, J. Phys. II (France) **51**, 2653 (1990).
[76] M. J. Bowick, S. M. Catterall, M. Falcioni, G. Thorleifsson, and K. N. Anagnostopoulos, The flat phase of crystalline membranes, J. Phys. I (France) **6**, 1321 (1996).
[77] M. Kastner, Phase transitions and configuration space topology, Rev. Mod. Phys. **80**, 167 (2008).
[78] J.-H. Kang, H. Kim, C. D. Santangelo, and R. C. Hayward, Enabling robust self-folding origami by pre-biasing vertex buckling direction, Adv. Mater. **31**, 0193006 (2019).
[79] J. Kästner, Umbrella sampling, WIREs Comput. Mol. Sci. **1**, 932 (2011).